

Understanding the Emergence of Multimodal Representation Alignment

Megan Tjandrasuwita¹ Chanakya Ekbote¹ Liu Ziyin¹ Paul Pu Liang¹

Abstract

Multimodal representation learning is fundamentally about transforming incomparable modalities into comparable representations. While prior research primarily focused on *explicitly* aligning these representations through targeted learning objectives and model architectures, a recent line of work has found that independently trained unimodal models of increasing scale and performance can become *implicitly* aligned with each other. These findings raise fundamental questions regarding the emergence of aligned representations in multimodal learning. Specifically: (1) when and why does alignment emerge implicitly? and (2) is alignment a reliable indicator of performance? Through a comprehensive empirical investigation, we demonstrate that both the emergence of alignment and its relationship with task performance depend on several critical data characteristics. These include, but are not necessarily limited to, the degree of similarity between the modalities and the balance between redundant and unique information they provide for the task. Our findings suggest that alignment may not be universally beneficial; rather, its impact on performance varies depending on the dataset and task. These insights can help practitioners determine whether increasing alignment between modalities is advantageous or, in some cases, detrimental to achieving optimal performance. Code is released at: https://github.com/MeganTj/multimodal_alignment.

1. Introduction

Multimodal AI represents a cutting-edge paradigm in machine learning that enables integrating and learning from many heterogeneous and interacting data modalities. These AI systems are revolutionizing predictive analytics across many applications, including in multimedia (Alayrac et al.,

¹Massachusetts Institute of Technology, USA. Correspondence to: Megan Tjandrasuwita <meganjt@mit.edu>.

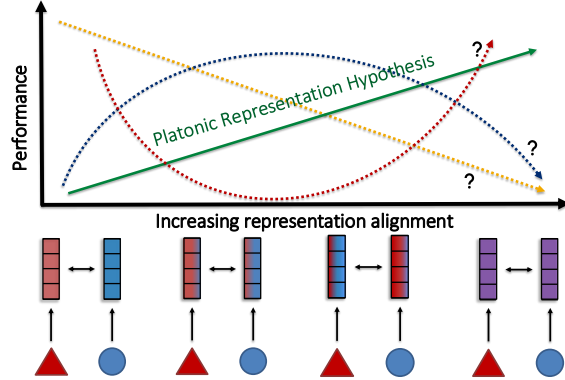


Figure 1: **Emergence of multimodal alignment?** While the Platonic Representation Hypothesis (Huh et al., 2024) argues that better alignment predicts better performance, our findings demonstrate that the relation between alignment and performance is more nuanced and depends on several dataset characteristics including the degree of heterogeneity and interactions between modalities.

2022; Sun et al., 2019; Ramesh et al., 2021; Singer et al., 2022), healthcare (Cai et al., 2019; Muhammad et al., 2021), and physical sensing (Kirchner et al., 2019; Lee et al., 2019; Xiao et al., 2020). A large body of research in designing and training multimodal models has focused on *aligning* the representations from different modalities such that they are comparable in some semantic representation space (Baltrušaitis et al., 2018; Liang et al., 2024). Conventional wisdom posits that aligned representations are a crucial precursor to multimodal fusion and representation learning (Li et al., 2021). As a result, many learning methods, such as contrastive learning and its variants (Frome et al., 2013; Jia et al., 2021; Radford et al., 2021a), and model architectures (Bertinetto et al., 2016; Lenc & Vedaldi, 2019; Bansal et al., 2021; Csiszárík et al., 2021) have been proposed to explicitly align incomparable modalities into comparable representation spaces for further processing.

However, recent work on the “Platonic Representation Hypothesis” showed that, surprisingly, alignment could even emerge across independently pre-trained vision and language models without explicitly aligning them together (Huh et al., 2024). Crucially, alignment increases with model size and performance, and it has been hypothesized that unimodal models will become increasingly

aligned. These findings raise fundamental questions regarding the emergence of aligned representations and their implications on multimodal learning: (1) when and why does alignment emerge implicitly, and (2) is alignment a reliable indicator of performance? We illustrate these open questions in Figure 1.

In this paper, we study these questions comprehensively across two principal dimensions that taxonomize multimodal data: *interactions* and *heterogeneity* (Baltrušaitis et al., 2018; Liang et al., 2024; Tian et al., 2020), visualized in Figure 2. Interactions measure the information shared between two modalities for a task, from more redundant (e.g., images and corresponding captions) to more unique (e.g., sensor placement). We expect alignment to emerge more easily between redundant modalities. Heterogeneity measures the degree of similarity across two modalities independent of the task, from more similar (e.g., two languages) to more different (e.g., text and video). We expect alignment to emerge more easily between similar modalities.

Through extensive experiments on controlled and real-world datasets with varying degrees of interactions and heterogeneity, we discover several key insights. First, the maximum alignment achievable depends on the degree of heterogeneity and uniqueness in the modalities, which inherently limits alignment. Second, while alignment correlates with performance in datasets with high redundancy, this relationship breaks down when uniqueness dominates redundancy. These findings highlight that performance often does not directly correspond to alignment, and the connection between them is a nuanced property of the data that varies across modalities and tasks. Therefore, our work provides important considerations for practitioners designing and training multimodal models, emphasizing that scale alone does not guarantee modality alignment and that careful assessment is necessary to determine when alignment is beneficial.

2. Representation Alignment

In this section, we review the concept of representation alignment through prior work on measuring alignment, methods to explicitly align representations, and observations regarding the emergence of alignment.

Measuring Alignment. Measuring alignment between neural network representations is a widely used approach in the research community to analyze and improve training dynamics (Huh et al., 2024; Klabunde et al., 2024; Kornblith et al., 2019). A prominent class of alignment metrics is based on canonical correlation analysis (CCA), a statistical technique for comparing two subspaces (Thompson, 2005; Golub & Zha, 1995), along with its nonlinear extensions using kernels (Lai & Fyfe, 2000; Raghu et al., 2017) and neural networks (Andrew et al., 2013; Wang et al., 2015;

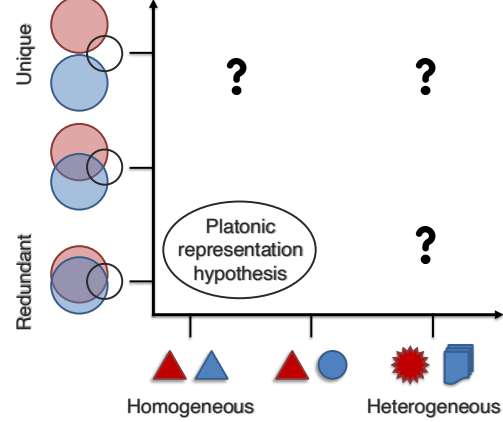


Figure 2: **Two principal dimensions of multimodal data.**

This study empirically evaluates data across two key dimensions: heterogeneity and interactions. Heterogeneity, represented on the x-axis, reflects the similarity between two data modalities regardless of the task, while interactions, on the y-axis, indicate the balance between redundant and unique task-relevant information across modalities. We expect the Platonic Representation Hypothesis to hold in cases of redundancy and similar modalities, but when and why alignment emerges implicitly, and whether alignment is a reliable indicator of performance, remain open questions.

Morcos et al., 2018). Among these methods, Kornblith et al. (2019) highlight the advantages of Centered Kernel Alignment (CKA), particularly its invariance to orthogonal transformations and isotropic scaling. Given mean-centered feature sets of n samples, $Z_1, Z_2 \in \mathbb{R}^{n \times d}$, from two modalities X_1 and X_2 , the CKA metric with a linear kernel is:

$$\text{CKA}(Z_1, Z_2) = \frac{\text{ALIGN}(Z_1, Z_2)}{\sqrt{\text{ALIGN}(Z_1, Z_1) \cdot \text{ALIGN}(Z_2, Z_2)}}$$

where $\text{ALIGN}(Z_1, Z_2)$ denotes $\text{HSIC}(Z_1 Z_1^\top, Z_2 Z_2^\top)$ with HSIC denoting an empirical estimator of the Hilbert-Schmidt Independence Criterion (Gretton et al., 2005). Intuitively, CKA quantifies alignment by comparing the covariance structures of two feature sets, capturing whether their representations encode similar relationships. This property ensures that even if Z_1 and Z_2 undergo arbitrary rotations (e.g., due to different initialization schemes), the CKA metric remains consistent, making it a robust choice for assessing representation alignment. For large vision-language models, given the high dimensionality and large embedding sizes of learned representations, we employ a computationally efficient variation of CKA — the mutual k-nearest neighbors (mutual KNN) method (Huh et al., 2024). Instead of directly comparing full covariance structures, this approach measures similarity by analyzing the overlap be-

tween the k-nearest neighbor sets of embeddings, improving scalability. Details are provided in Appendix B.

Explicit Alignment. In addition to research on measuring alignment in neural networks, another line of work focuses on explicitly aligning representations, a widely used technique for handling heterogeneous modalities (Liang et al., 2024). A popular approach in this domain is multimodal contrastive learning, where representations of the same concept across different modalities (i.e., positive pairs) are brought closer together, while representations of different concepts (i.e., negative pairs) are pushed apart (Frome et al., 2013; Jia et al., 2021; Radford et al., 2021a). The coordination distance in contrastive learning is typically measured using cosine distance (Mekhaldi, 2007) or max-margin losses (Hu et al., 2019). Theoretical results demonstrate that contrastive learning effectively captures redundant information shared between modalities (Tian et al., 2020; Tosh et al., 2021). More recent extensions have been proposed to also capture unique and synergistic information, further refining multimodal representation learning (Dufumier et al., 2024; Liang et al., 2023b).

Emergence of Implicit Alignment. In contrast to explicit alignment methods, recent findings suggest that alignment can emerge implicitly, even when neural networks differ in training objectives, datasets, and architectures (Li et al., 2015; Raghu et al., 2017; Lenc & Vedaldi, 2019; Baranikov et al., 2022; Bonheme & Grzes, 2022). Notably, this similarity becomes more pronounced in larger and wider networks (Raghu et al., 2017; Morcos et al., 2018; Kornblith et al., 2019). Building on the observation that latent spaces are inherently comparable, a line of research explores composing components of different models with minimal or no additional training. Lenc & Vedaldi (2019) demonstrate that latent spaces can be stitched together using trainable stitching layers, while subsequent studies (Bansal et al., 2021; Csiszárík et al., 2021) show that better-performing models tend to learn more similar representations when stitched. More recently, the Platonic Representation Hypothesis (Huh et al., 2024) suggests that as vision and language models scale in capacity and performance, independently trained models exhibit increasing alignment. This finding implies that models are converging toward modality-agnostic representations, reinforcing the idea that alignment may emerge naturally as a byproduct of model scaling. However, if alignment continues to emerge, there would be no need for any of the explicit alignment methods described above. That explicit alignment has consistently been helpful implies either emergent alignment is not sufficient or emergent alignment does not always lead to improved performance. This discrepancy between the possibility of emergent alignment and the need for explicit alignment methods calls for a systematic exploration of the role of alignment and its downstream

relationship to performance in multimodal learning.

3. Research Questions and Experimental Setup

The recent line of work on the emergence of alignment across independently pre-trained unimodal models raises fundamental questions regarding the emergence of aligned representations and their implications on multimodal learning. Our research seeks to understand (1) when and why alignment emerges implicitly, and (2) whether alignment is a reliable indicator of performance. To reliably and comprehensively study these questions across all types of multimodal data, we use two principle dimensions to taxonomize multimodal data: *interactions* and *heterogeneity* (Baltrušaitis et al., 2018; Liang et al., 2024; Tian et al., 2020). Interactions measure the information shared between two modalities for a task, from more redundant (e.g., images and corresponding captions) to more unique (e.g., sensor placement). We expect alignment to emerge more easily between redundant modalities. Heterogeneity measures the degree of similarity across two data modalities independent of the task, from more similar (e.g., two languages) to more different (e.g., text and video). We expect alignment to emerge more easily between similar modalities. Our experiments aim to study the emergence of alignment and its relationship to downstream task performance by systematically varying the interactions and heterogeneity in multimodal data. To summarize, our fundamental guiding questions are:

1. Does alignment emerge when uniqueness and heterogeneity increase?
2. Does higher alignment always predict better performance when uniqueness is present?
3. How can we characterize datasets through the correlation between performance and alignment?

Based on these questions, we define our problem setting.

3.1. Problem Setting

We focus on a simplified setting with two modalities and an associated label, the generalization is straightforward. Concretely, we consider a scenario where we sample multimodal data and labels $x_1, x_2, y \sim \mathbb{P}(X_1, X_2, Y)$ from a data distribution $\mathbb{P}(X_1, X_2, Y)$. X_i represents the random variable for the i -th modality and Y for the task. Based on the relationships between X_1 , X_2 , and Y , these modalities can exhibit different degrees of interactions and heterogeneity.

Interactions measure the information shared between two modalities for a task, from more redundant to more unique. Redundancy R represents the shared information between the two modalities and the task (Y), such as between images and captions that describe the image (Radford et al., 2021a). Uniqueness in modality 1 (U_1) quantifies the amount of information present in the first modality absent in the sec-

ond but critical for the downstream task (and likewise for U_2). For example, feature selection is often optimized to provide new unique information and minimize redundancy to previous ones (Peng et al., 2005).

To investigate how alignment and performance change with respect to different interactions, we need synthetic controllable datasets and real-world multimodal benchmarks with different interactions. For constructing synthetic data, we assume that the task-relevant information (for a particular label y) can be decomposed into x_r, x_{u_1}, x_{u_2} , where x_r denotes the common or redundant information, x_{u_1} represents information unique to the first modality, and x_{u_2} captures information unique to the second modality.

We construct the input data as $x_1 = [x_r, x_{u_1}]$ and $x_2 = [x_r, x_{u_2}]$. An overview of the data generation process is shown in Figure 3. By selecting specific features to compute the label, we control the levels of redundancy and uniqueness. Specifically, Y is a nonlinear function of a subset of features, $\mathcal{S} \subseteq [x_r, x_{u_1}, x_{u_2}]$. This enables us to control R as the number of features in \mathcal{S} that come from x_r , and U_i as the number of features that come from x_{u_i} for $i \in \{1, 2\}$. We denote the total uniqueness $U = |\mathcal{S}| - R$. By keeping $|\mathcal{S}|$ fixed while varying U , we generate datasets with different proportions of redundant versus non-redundant information.

Heterogeneity. Different modalities often exhibit distinct structures, qualities, and representations (Liang et al., 2024). For example, when one modality is a time series and another is a static image, differences in their vocabulary tokens, and different noise or distribution shifts in each modality. We aim to investigate how alignment and performance change with different degrees of heterogeneity, from more similar (e.g., two languages) to more different (e.g., text and video).

To generate synthetic datasets with varying heterogeneity, we start with the case where both modalities are redundant, meaning Y (the labels) is a nonlinear function of x_r . Specifically, let $x_1 = x_r$ and $x_2 = \phi(x_r)$, where $\phi(\cdot)$ is a nonlinear bijective function, as shown in Figure 3. In this setting, heterogeneity is defined as the number of nonlinear transformations involved in $\phi(\cdot)$. Concretely, if $\phi(\cdot)$ is modeled as a multilayer perceptron (MLP), the number of layers D_ϕ quantifies the level of heterogeneity between the two modalities. We extend this definition to cases where the modalities contain unique information. Let x_r represent the shared information between the two modalities, and x_{u_1} and x_{u_2} denote the unique information in each modality. In this scenario, $X_1 = [x_r, x_{u_1}]$, and a modality that is heterogeneous with respect to X_1 is defined as $X_2 = \phi([x_r, x_{u_2}])$. Here, we assume ϕ is a bijection, ensuring that the information content of X_2 and $[x_r, x_{u_2}]$ remains unchanged.

Experimental setup for synthetic datasets. We evaluate how uniqueness, redundancy, and heterogeneity influence

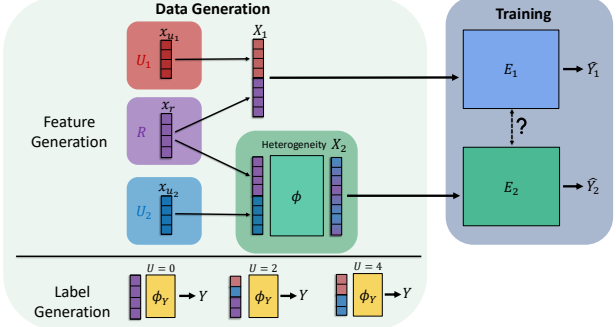


Figure 3: Synthetic data generation and training. We generate synthetic data with varying levels of uniqueness and heterogeneity. The building blocks are the redundant and unique components $[x_r, x_{u_1}, x_{u_2}]$, where $[x_r, x_{u_1}]$ are used in creating X_1 and $[x_r, x_{u_2}]$ are for X_2 . The level of uniqueness is determined by the number of features from x_r that are used to compute the labels Y , given that the total number of features used for label computation is held constant. X_2 is transformed into a heterogeneous modality using a transformation network ϕ . In our experiments, we compute alignment between unimodal encoders E_1, E_2 trained on X_1, X_2 respectively.

the emergence of alignment by training encoders independently on each modality and measuring the alignment between their learned representations. Specifically, we train a single-layer encoder on the first modality, denoted as E_1 . For the second modality, which is transformed by the nonlinear function $\phi(\cdot)$ with varying depths (D_ϕ), we train a series of encoders denoted as $E_{2,D_{Enc}}$, where D_{Enc} represents the depth of the encoder trained on the second modality and varies as $D_{Enc} \in \{1, \dots, 10\}$.

Experimental setup for real benchmarks. In addition to experiments on synthetic data, we conduct analogous experiments on vision-language models. We use the same dataset and models as Huh et al. (2024), which evaluates alignment on the Wikipedia caption dataset (Srinivasan et al., 2021) with naturally co-occurring text and images. This dataset is inherently heterogeneous (text and images are different) with high redundancy due to overlapping semantic information. To vary the amount of unique information, we introduce a preprocessing procedure that perturbs the data in each modality. Specifically, for text, we randomly delete a percentage of characters, reducing the amount of information available in the textual representation. For image data, we replace a certain percentage of pixels with values drawn from a Gaussian distribution that matches the mean and variance of the original image.

Finally, we experiment with MultiBench (Liang et al., 2021b) which collects a diverse range of real-world multimodal datasets: MOSEI (Bagher Zadeh et al., 2018), a

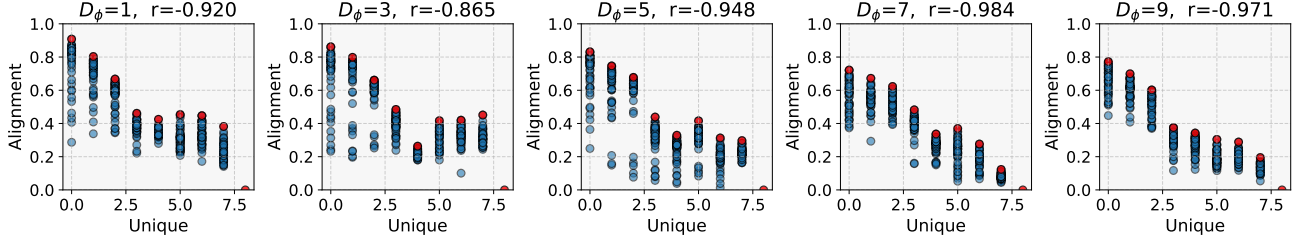


Figure 4: **Alignment vs uniqueness on synthetic datasets.** The alignment is computed between unimodal encoders trained on datasets with different levels of informational uniqueness. Each dot is an independent run on a different model size on a given dataset. We see that the maximum level of achievable level of alignment decreases as the level of uniqueness increases. Five different figures shows the different levels of nonlinear transformation we apply to the original data.

dataset for predicting emotions from videos (vision, audio, language); MOSI (Zadeh et al., 2016), a dataset for predicting sentiment from videos (vision, audio, language), URFUNNY (Hasan et al., 2019), a humor detection dataset from videos (vision, audio, language); MUStARD (Castro et al., 2019), a sarcasm detection dataset from TV shows (vision, audio, language); and AVMNIST (Pérez-Rúa et al., 2019), a dataset for digit classification from paired images and spoken digits. While we cannot explicitly vary the information content, past work has collected human annotations of the levels of redundancy and uniqueness in these datasets, showing that most multimodal datasets have a significant amount of uniqueness (Liang et al., 2023a).

Computing Alignment. For models trained on synthetic data, we evaluate alignment using Centered Kernel Alignment (CKA) (Kornblith et al., 2019). Following the methodology outlined in Huh et al. (2024), we evaluate alignment using mutual KNN, a variant of CKA. See Appendix B for more details.

4. RQ1: When does Alignment Emerge?

We empirically evaluate whether alignment emerges naturally by systematically varying redundancy, uniqueness, and heterogeneity. In the synthetic setting, the level of uniqueness U denotes the number of unique features used in computing the label. In Figure 4, we observe that as U increases, the maximum alignment decreases across different model depths and transformation depths. A similar trend is evident in Figure 5, which examines the alignment between large-scale language models and DINOv2 (Oquab et al., 2023) vision models over different levels of U is the percentage of perturbation. See Appendix D.2 for experiments with more vision models. An additional experiment, detailed in Appendix D.1, demonstrates that data heterogeneity is negatively correlated with the level of achievable alignment. Collectively, these experiments provide strong empirical evidence supporting the hypothesis that the level of alignment is indeed constrained by the degrees of heterogeneity and

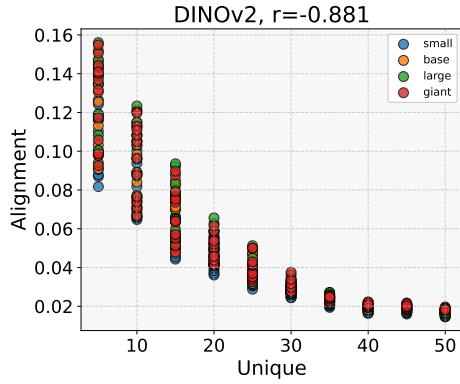


Figure 5: **Alignment vs uniqueness on real large-scale vision-language datasets.** Alignment is computed between DINOv2 vision models and large language models. Each dot is an independent run on a different model size on a dataset with a given level of uniqueness. The maximum achievable alignment decreases as uniqueness increases.

interactions between the modalities.

We now investigate whether increasing model capacity can improve alignment between representations of increasingly heterogeneous and unique modalities. In Figure 6, we plot alignment scores as a function of (D_{Enc}, D_ϕ) , where D_{Enc} represents the encoder depth and D_ϕ represents the transformation depth of the second modality. When uniqueness is low, we observe that alignment improves significantly when the model capacity (relative to the transformation depth) is greater. This suggests that increased model capacity is effective in handling heterogeneity between modalities. Concretely, in these scenarios, alignment appears to follow the trend $(D_{Enc} - D_\phi) \propto \text{Alignment}$, meaning that the relative capacity of the encoder compensates for the complexity introduced by the transformation depth. However, as uniqueness increases, the relationship between alignment and relative model capacity becomes much weaker. In these cases, $(D_{Enc} - D_\phi)$ no longer predicts higher alignment scores. This indicates that when modalities have a high level

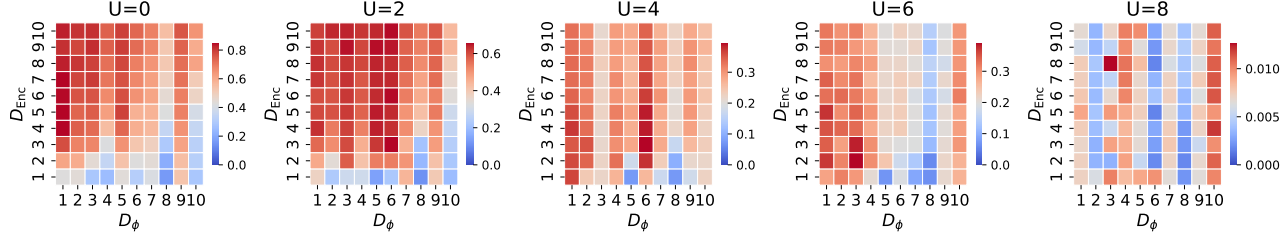


Figure 6: **Emergence of alignment across heterogeneity and uniqueness.** We plot alignment over increasing unimodal encoder depths for the transformed modality and different levels of heterogeneity. When redundancy is high, we see that alignment emerges when $(D_{Enc} - D_{\phi})$ is high. However, as uniqueness increases, the relationship between $(D_{Enc} - D_{\phi})$ and alignment is much weaker.

of unique information, simply increasing model capacity is insufficient to achieve higher alignment. Instead, other factors—such as the degree of shared information—may become the limiting factor in determining alignment.

In summary, while model size and capacity are correlated with alignment, there exists an upper limit to the level of achievable alignment, which is fundamentally determined by the intrinsic properties of the data. This finding implies that perfect alignment cannot be simultaneously achieved with optimal performance when the data modalities inherently differ in their information content. Moreover, increasing model depth only effectively aligns heterogeneous modalities when they contain highly redundant information and can fail for high uniqueness.

5. RQ2: Is Alignment Correlated with Performance?

In this section, we systematically investigate the relationship between alignment and performance, identifying scenarios where alignment enhances performance and others where it may introduce unintended trade-offs.

5.1. Alignment-performance vs interactions/uniqueness

For each synthetic dataset, we analyze the relationship between alignment, performance, and model capacity. We include model capacity in our analysis as increased capacity generally leads to better performance and is assumed to correlate with better alignment. Our findings are summarized in Figure 7, where we plot the correlations between alignment and performance across different dataset dimensions, where U is defined in Section 4. In highly redundant settings, the correlation between alignment and performance is strong, with relatively little variation across different levels of heterogeneity and random seeds. However, as uniqueness increases, the median correlation decreases toward zero, and the range of correlations expands significantly. Notably, for $U > 3$, the correlation even becomes negative in some cases, suggesting that higher uniqueness can disrupt

the relationship between alignment and performance. A similar trend is observed when examining the correlation between alignment and model depth in Figure 7 (right). As uniqueness increases, both the median correlation decreases and the variance in correlation increases substantially, with instances of anticorrelated alignment-depth relationships. While deeper models do not necessarily lead to better alignment when uniqueness is high, we see in Figure 7 (center) that performance and depth remain positively correlated across different levels of uniqueness, with much lower variance in correlation at higher uniqueness levels. This suggests that while alignment may not always be a reliable predictor of performance, increasing model capacity can still improve task performance.

We next verify whether these findings extend to large vision-language models. In Figure 8, we observe a strong correlation between alignment to DINOv2 and language model performance when uniqueness is low. However, this relationship weakens as uniqueness increases. By $U = 25$, models with lower alignment outperform those with higher alignment. As uniqueness increases further, the correlation between alignment and performance largely disappears. Additionally, we find that higher-performing language models are not necessarily those with greater capacity. This suggests that alignment and model size alone may not guarantee better performance in high-uniqueness settings. We include more analysis in Appendix D.3 involving different vision model training schemes. Overall, our experiments on both synthetic data and large vision-language models indicate that as uniqueness increases, higher-performing models with greater capacity do not necessarily exhibit stronger alignment. This reinforces the conclusion that alignment does not always predict model effectiveness, particularly when the modalities contain significant amounts of unique information.

5.2. Alignment-performance vs heterogeneity

Additionally, we analyze whether alignment correlates with performance across varying levels of heterogeneity in Fig-

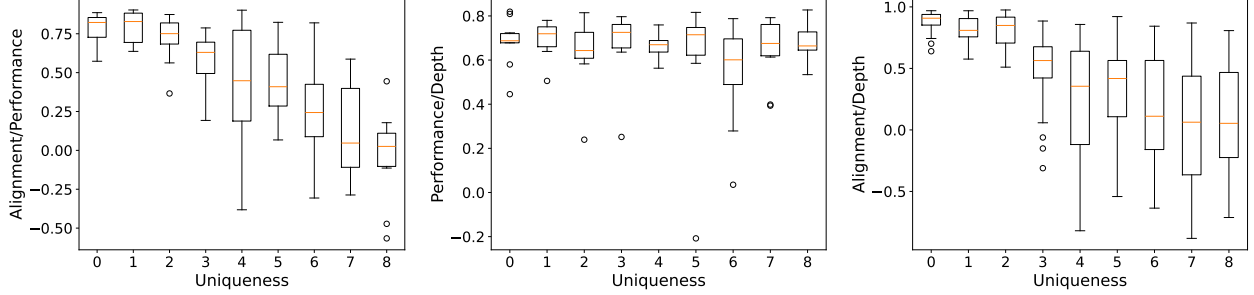


Figure 7: **Alignment, performance, and depth correlation plots across different synthetic depths and experiment seeds.**

In each plot, we show the spread of Pearson correlation coefficients for each level of uniqueness, where the orange lines are the median correlations and the dots are outliers. **Left:** When the two modalities are fully redundant, the alignment is strongly correlated with performance. When the two modalities have high uniqueness, alignment has a vanishing correlation with performance. In fact, for a significant proportion of tasks, the correlation is negative. **Mid:** In contrast, model size measured by depth always has a strong positive correlation with performance and does not seem to change across datasets. This means that representation alignment may not be a universal phenomenon, and is introduced by some special properties of data. In contrast, the influence of model size on performance seems universal and is consistent with the well-observed scaling laws. **Right:** For each level of uniqueness, we show the variance in alignment/depth correlation. As uniqueness increases, the median alignment/depth decreases to 0, and the range of correlation values increases significantly.

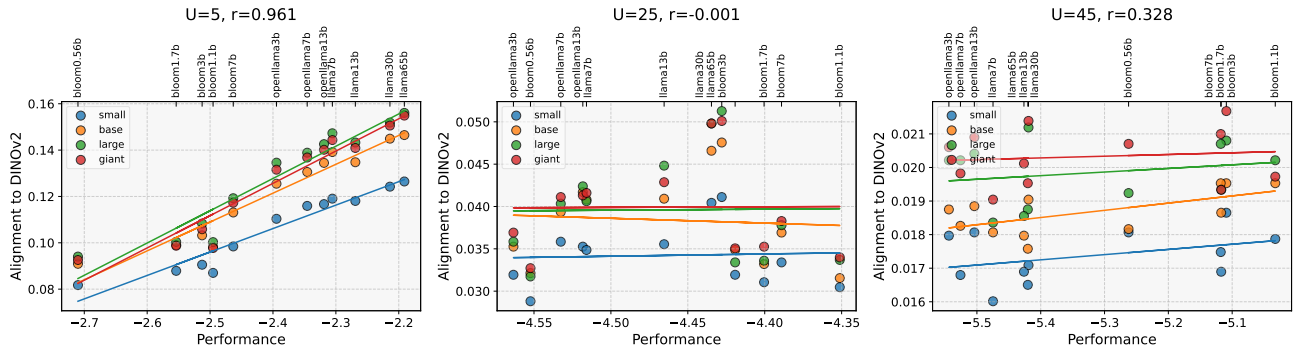


Figure 8: **Alignment vs performance across different uniqueness.** We plot the vision-language alignment using DINOv2 vision models with respect to language model performance, measured using negative bits-per-byte-loss. We show individual best fit lines for each size of vision model and the average Pearson correlation coefficient r . At $U = 5$, we see that model performance highly correlates with model capacity. However, at $U = 25$ and $U = 45$, the correlation vanishes, and the best performing models are not those with most capacity, as smaller bloom models outperform all other models.

ure 9. Intuitively, we expect higher levels of heterogeneity to result in lower performance, but it is unclear whether this trend is reflected in alignment scores. Our findings show that while alignment and performance exhibit a strong linear relationship at low levels of uniqueness, this relationship weakens as uniqueness increases. Specifically, with higher uniqueness, models trained on similar modalities do not consistently achieve better alignment than those trained on heterogeneous modalities. This suggests that alignment does not uniformly degrade with increasing heterogeneity and that the interaction between uniqueness, heterogeneity, and alignment is more complex than a simple linear relationship. These results further reinforce the idea that alignment alone is not a sufficient predictor of model performance, especially in multimodal settings where modalities contain

varying levels of interactions and heterogeneity.

6. RQ3: Alignment-Performance Correlation is an Inherent Property of Datasets

Finally, we investigate how the alignment-performance correlation varies across real-world multimodal datasets. Quantifying this relation is important to practitioners, as a positive alignment-performance correlation suggests that a practitioner can improve performance by explicitly aligning modalities. As shown in our experiments in Section 5, we expect that on tasks involving redundant information, alignment positively correlates with performance whereas for tasks that require unique information in modalities, the correlation may be weaker and not necessarily positive.

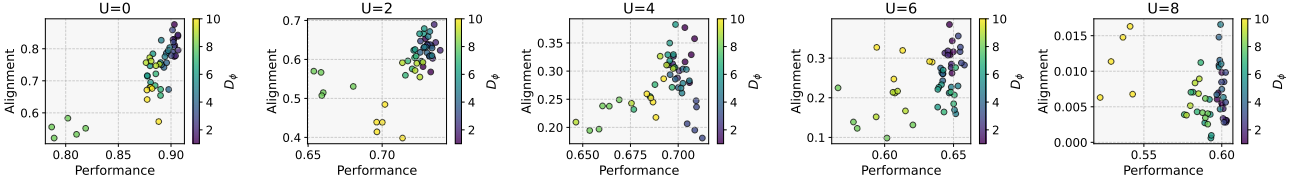


Figure 9: **Alignment vs performance across levels of heterogeneity.** We plot the alignment and performance scores at different levels of heterogeneity, with the transformed modality’s encoder fixed to the maximum transformation depth. At high levels of uniqueness, we see that high performance correlates with high alignment, with both being greater at lower synthetic depths. Past $U = 4$, we see that while performance is higher at lower synthetic depths, the alignment scores on these datasets are not necessarily higher.

Dataset	Vision - Audio		Vision - Text		Audio - Text	
	Vision	Audio	Vision	Text	Audio	Text
MOSEI (Bagher Zadeh et al., 2018)	-0.193	-0.154	-0.154	-0.351	-0.158	-0.366
MOSI (Zadeh et al., 2016)	-0.135	0.249	0.092	-0.336	0.291	-0.374
URFUNNY (Hasan et al., 2019)	-0.384	-0.369	-0.327	0.347	-0.380	0.074
MUStARD (Castro et al., 2019)	0.404	0.180	0.530	0.014	0.139	0.458
AVMNIST (Pérez-Rúa et al., 2019)	0.944	0.974	-	-	-	-

Table 1: **Alignment-performance correlations on MultiBench.** We compute the correlation between model performance and alignment across 4 affective computing datasets with tasks that require unique information in vision, audio, and language modalities. We additionally benchmark on AVMNIST, a dataset with high redundancy as the modalities are images of digits and spoken digits for digit classification. On the affective computing datasets, the correlation is weak and often negative, suggesting that enforcing alignment between modalities may not be desirable. In contrast, the alignment of vision and audio modalities in AVMNIST is highly correlated with performance.

We evaluate these hypotheses on a subset of datasets from MultiBench (Liang et al., 2021a) with varying degrees of task-relevant redundant and unique information content, including MOSEI (Bagher Zadeh et al., 2018), a dataset for predicting emotions from videos (vision, audio, text); MOSI (Zadeh et al., 2016), a dataset for predicting sentiment from videos (vision, audio, text), URFUNNY (Hasan et al., 2019), a humor detection dataset from videos (vision, audio, text); MUSTARD (Castro et al., 2019), a sarcasm detection dataset from TV shows (vision, audio, text); and AVMNIST (Pérez-Rúa et al., 2019), a dataset for digit classification from paired images and spoken digits (vision, audio). See Appendix C.2 for details about the datasets. For each modality, we train transformers with varying depths and compute the cross-modal alignment. See Appendix A for details on our experiment setup.

We show these results in Table 1. On sentiment analysis tasks that typically require unique information from language, alignment and performance are weakly correlated or even negatively correlated. For a given dataset, the alignment-performance relationship can even vary between different modalities. For example, on MUStARD, alignment is more highly correlated with vision performance, whereas audio and text performance do not seem as correlated. On AVMNIST, alignment strongly correlates with performance for both modalities, as the information content is largely redundant information about the digit identity. These results

corroborate our findings that the alignment-performance relationship heavily depends on dataset characteristics.

7. Conclusion

This paper provides a comprehensive analysis of the relationship between multimodal alignment, performance, and multimodal data characteristics. We offer a nuanced perspective on how alignment emerges across different modalities and how its effectiveness is influenced by the interactions and heterogeneity within the data. Specifically, our findings show that as uniqueness and heterogeneity increase, the emergence of alignment weakens, and that alignment often fails to track performance in datasets with higher uniqueness. In the case of perfect redundancy, our result supports the Platonic Representation Hypothesis, but as the amount of unique information and data heterogeneity increases, our results provide a generalization of this phenomenon.

Our work opens up the possibility of characterizing and quantifying multimodal datasets via alignment-performance relationships. This can help advance our understanding of multimodal data and inspire the design of better methods that appropriately align (or perhaps even unalign) modality representations when necessary. Our work also inspires new theoretical questions regarding why different models sometimes converge to similar representations, even though they are often overparametrized and theoretically capable

of learning arbitrary representations. Answering these questions can advance our understanding of today’s large-scale multimodal AI systems.

Impact Statement

This paper presents an empirical analysis whose goal is to advance the field of multimodal representation learning. Multimodal models are broadly impactful for many real-world applications including understanding human verbal and nonverbal communication, fusing multiple physical sensors, and analyzing multiple sources of medical data. There are many potential long-term societal consequences of our work, but since our work is primarily an empirical analysis, we feel that none of these impacts must be specifically highlighted here.

Acknowledgements

MT is supported by the National Science Foundation (NSF) under Grant No. 2141064. We thank Hengzhi Li and Min-seok Jung for feedback and discussions.

References

Alayrac, J.-B., Donahue, J., Luc, P., Miech, A., Barr, I., and Hasson, Y. Flamingo: a visual language model for few-shot learning. *arXiv preprint arXiv:2204.14198*, 2022.

Andrew, G., Arora, R., Bilmes, J., and Livescu, K. Deep canonical correlation analysis. In *ICML*, 2013.

Bagher Zadeh, A., Liang, P. P., Poria, S., Cambria, E., and Morency, L.-P. Multimodal Language Analysis in the Wild: CMU-MOSEI Dataset and Interpretable Dynamic Fusion Graph. In Gurevych, I. and Miyao, Y. (eds.), *Proceedings of the 56th Annual Meeting of the Association for Computational Linguistics (Volume 1: Long Papers)*, pp. 2236–2246, Melbourne, Australia, July 2018. Association for Computational Linguistics. doi: 10.18653/v1/P18-1208. URL <https://aclanthology.org/P18-1208/>.

Baltrušaitis, T., Ahuja, C., and Morency, L.-P. Multimodal machine learning: A survey and taxonomy. *IEEE TPAMI*, 41(2):423–443, 2018.

Bansal, Y., Nakkiran, P., and Barak, B. Revisiting Model Stitching to Compare Neural Representations, June 2021. URL <https://arxiv.org/abs/2106.07682>. arXiv:2106.07682.

Barannikov, S., Trofimov, I., Balabin, N., and Burnaev, E. Representation Topology Divergence: A Method for Comparing Neural Network Representations. In *Proceedings of the 39th International Conference on Machine Learning*, pp. 1607–1626. PMLR, June 2022. URL <https://proceedings.mlr.press/v162/barannikov22a.html>. ISSN: 2640-3498.

Bertinetto, L., Valmadre, J., Henriques, J. F., Vedaldi, A., and Torr, P. H. Fully-convolutional siamese networks for object tracking. In *Computer Vision–ECCV 2016 Workshops: Amsterdam, The Netherlands, October 8–10 and 15–16, 2016, Proceedings, Part II* 14, pp. 850–865. Springer, 2016.

Bonheme, L. and Grzes, M. How do Variational Autoencoders Learn? Insights from Representational Similarity, September 2022. URL <http://arxiv.org/abs/2205.08399>. arXiv:2205.08399 [cs].

Cai, Q., Wang, H., Li, Z., and Liu, X. A survey on multimodal data-driven smart healthcare systems: approaches and applications. *IEEE Access*, 7:133583–133599, 2019.

Castro, S., Hazarika, D., Pérez-Rosas, V., Zimmermann, R., Mihalcea, R., and Poria, S. Towards Multimodal Sarcasm Detection (An _obviously_ Perfect Paper). In Korhonen, A., Traum, D., and Márquez, L. (eds.), *Proceedings of the 57th Annual Meeting of the Association for Computational Linguistics*, pp. 4619–4629, Florence, Italy, July 2019. Association for Computational Linguistics. doi: 10.18653/v1/P19-1455. URL <https://aclanthology.org/P19-1455/>.

Csiszárík, A., KHorösi-Szabó, P., Matszangosz, A., Papp, G., and Varga, D. Similarity and Matching of Neural Network Representations. In *Advances in Neural Information Processing Systems*, volume 34, pp. 5656–5668. Curran Associates, Inc., 2021. URL <https://proceedings.neurips.cc/paper/2021/hash/2cb274e6ce940f47beb8011d8ecb1462-Abstract.html>.

Dufumier, B., Castillo-Navarro, J., Tuia, D., and Thiran, J.-P. What to align in multimodal contrastive learning?, September 2024. URL <http://arxiv.org/abs/2409.07402>. arXiv:2409.07402 [cs].

Frome, A., Corrado, G. S., Shlens, J., Bengio, S., Dean, J., Ranzato, M., and Mikolov, T. Devise: A deep visual-semantic embedding model. In *Advances in neural information processing systems*, pp. 2121–2129, 2013.

Geng, X. and Liu, H. OpenLLaMA: An Open Reproduction of LLaMA, May 2023. URL https://github.com/openlm-research/open_llama.

Golub, G. H. and Zha, H. *The canonical correlations of matrix pairs and their numerical computation*. Springer, 1995.

Gretton, A., Bousquet, O., Smola, A., and Schölkopf, B. Measuring statistical dependence with hilbert-schmidt norms. In *International conference on algorithmic learning theory*, pp. 63–77. Springer, 2005.

Hasan, M. K., Rahman, W., Bagher Zadeh, A., Zhong, J., Tanveer, M. I., Morency, L.-P., and Hoque, M. E. UR-FUNNY: A Multimodal Language Dataset for Understanding Humor. In Inui, K., Jiang, J., Ng, V., and Wan, X. (eds.), *Proceedings of the 2019 Conference on Empirical Methods in Natural Language Processing and the 9th International Joint Conference on Natural Language Processing (EMNLP-IJCNLP)*, pp. 2046–2056, Hong Kong, China, November 2019. Association for Computational Linguistics. doi: 10.18653/v1/D19-1211. URL <https://aclanthology.org/D19-1211/>.

He, K., Chen, X., Xie, S., Li, Y., Dollár, P., and Girshick, R. Masked Autoencoders Are Scalable Vision Learners. In *Proceedings of the IEEE/CVF Conference on Computer Vision and Pattern Recognition*, pp. 16000–16009, 2022.

Hu, D., Nie, F., and Li, X. Deep multimodal clustering for unsupervised audiovisual learning. In *CVPR*, pp. 9248–9257, 2019.

Huh, M., Cheung, B., Wang, T., and Isola, P. The Platonic Representation Hypothesis, July 2024. URL <http://arxiv.org/abs/2405.07987>. arXiv:2405.07987.

Jackson, Z. Jakobovski/free-spoken-digit-dataset, January 2025. URL <https://github.com/Jakobovski/free-spoken-digit-dataset>. original-date: 2016-06-21T09:46:20Z.

Jia, C., Yang, Y., Xia, Y., Chen, Y.-T., Parekh, Z., and Pham, H. Scaling up visual and vision-language representation learning with noisy text supervision. In *ICML*, pp. 4904–4916. PMLR, 2021.

Kirchner, E. A., Fairclough, S. H., and Kirchner, F. *Embedded multimodal interfaces in robotics: applications, future trends, and societal implications*, pp. 523–576. Association for Computing Machinery and Morgan & Claypool, 2019. ISBN 9781970001754. URL <https://doi.org/10.1145/3233795.3233810>.

Klabunde, M., Schumacher, T., Strohmaier, M., and Lemmerich, F. Similarity of Neural Network Models: A Survey of Functional and Representational Measures, August 2024. URL <http://arxiv.org/abs/2305.06329>. arXiv:2305.06329 [cs].

Kornblith, S., Norouzi, M., Lee, H., and Hinton, G. Similarity of Neural Network Representations Revisited, July 2019. URL <http://arxiv.org/abs/1905.00414>. arXiv:1905.00414.

Lai, P. L. and Fyfe, C. Kernel and nonlinear canonical correlation analysis. *International journal of neural systems*, 10(05):365–377, 2000.

Lecun, Y., Bottou, L., Bengio, Y., and Haffner, P. Gradient-based learning applied to document recognition. *Proceedings of the IEEE*, 86(11):2278–2324, November 1998. ISSN 1558-2256. doi: 10.1109/5.726791. URL <https://ieeexplore.ieee.org/document/726791>. Conference Name: Proceedings of the IEEE.

Lee, M. A., Zhu, Y., Srinivasan, K., Shah, P., and Savarese, S. Making sense of vision and touch: Self-supervised learning of multimodal representations for contact-rich tasks. In *ICRA*, pp. 8943–8950. IEEE, 2019.

Lenc, K. and Vedaldi, A. Understanding Image Representations by Measuring Their Equivariance and Equivalence. *Int. J. Comput. Vision*, 127(5):456–476, May 2019. ISSN 0920-5691. doi: 10.1007/s11263-018-1098-y. URL <https://doi.org/10.1007/s11263-018-1098-y>.

Li, J., Selvaraju, R., Gotmare, A., Joty, S., Xiong, C., and Hoi, S. C. H. Align before fuse: Vision and language representation learning with momentum distillation. *Advances in neural information processing systems*, 34:9694–9705, 2021.

Li, Y., Yosinski, J., Clune, J., Lipson, H., and Hopcroft, J. Convergent Learning: Do different neural networks learn the same representations? In *Proceedings of the 1st International Workshop on Feature Extraction: Modern Questions and Challenges at NIPS 2015*, pp. 196–212. PMLR, December 2015. URL <https://proceedings.mlr.press/v44/li15convergent.html>. ISSN: 1938-7228.

Liang, P. P., Lyu, Y., Fan, X., Wu, Z., Cheng, Y., Wu, J., and Chen, L. Y. Multibench: Multiscale benchmarks for multimodal representation learning. In *NeurIPS Datasets and Benchmarks Track*, 2021a.

Liang, P. P., Lyu, Y., Fan, X., Wu, Z., Cheng, Y., Wu, J., Chen, L. Y., Wu, P., Lee, M. A., Zhu, Y., Salakhutdinov, R., and Morency, L.-P. MultiBench: Multiscale Benchmarks for Multimodal Representation Learning. *Proceedings of the Neural Information Processing Systems Track on Datasets and Benchmarks*, 1, December 2021b. URL <https://datasets-benchmarks-proceedings.neurips.cc/paper/2021/hash/37693cf748049e45d87b8c7d8b9aacd-Abstract-round1.html>.

Liang, P. P., Cheng, Y., Fan, X., Ling, C. K., Nie, S., Chen, R. J., and Deng, Z. Quantifying & modeling multimodal interactions: An information decomposition framework. In *NeurIPS*, 2023a.

Liang, P. P., Deng, Z., Ma, M., Zou, J., Morency, L.-P., and Salakhutdinov, R. Factorized contrastive learning: Going beyond multi-view redundancy. In *NeurIPS*, 2023b.

Liang, P. P., Zadeh, A., and Morency, L.-P. Foundations & trends in multimodal machine learning: Principles, challenges, and open questions. *ACM Computing Surveys*, 56(10):1–42, 2024.

McFee, B., Raffel, C., Liang, D., Ellis, D. P., McVicar, M., Battenberg, E., and Nieto, O. librosa: Audio and music signal analysis in python. In *Proceedings of the 14th python in science conference*, volume 8, 2015.

Mekhaldi, D. Multimodal document alignment: towards a fully-indexed multimedia archive. In *Proceedings of the Multimedia Information Retrieval Workshop, SIGIR, Amsterdam, the Netherlands*, 2007.

Morcos, A. S., Raghu, M., and Bengio, S. Insights on representational similarity in neural networks with canonical correlation, October 2018. URL <http://arxiv.org/abs/1806.05759>. arXiv:1806.05759 [stat].

Muhammad, G., Alshehri, F., Karray, F., and El Saddik, A. A comprehensive survey on multimodal medical signals fusion for smart healthcare systems. *Information Fusion*, 76:355–375, 2021.

Quab, M., Darct, T., Moutakanni, T., Vo, H. V., Szafraniec, M., Khalidov, V., Fernandez, P., Haziza, D., Massa, F., El-Nouby, A., Assran, M., Ballas, N., Galuba, W., Howes, R., Huang, P.-Y., Li, S.-W., Misra, I., Rabbat, M., Sharma, V., Synnaeve, G., Xu, H., Jegou, H., Mairal, J., Labatut, P., Joulin, A., and Bojanowski, P. DINOv2: Learning Robust Visual Features without Supervision. *Transactions on Machine Learning Research*, July 2023. ISSN 2835-8856. URL <https://openreview.net/forum?id=a68SUt6zFt>.

Peng, H., Long, F., and Ding, C. Feature selection based on mutual information criteria of max-dependency, max-relevance, and min-redundancy. *IEEE Transactions on pattern analysis and machine intelligence*, 27(8):1226–1238, 2005.

Pérez-Rúa, J.-M., Vielzeuf, V., Pateux, S., Baccouche, M., and Jurie, F. Mfas: Multimodal fusion architecture search. In *CVPR*, pp. 6966–6975, 2019.

Pérez-Rúa, J.-M., Vielzeuf, V., Pateux, S., Baccouche, M., and Jurie, F. MFAS: Multimodal Fusion Architecture Search, March 2019. URL <http://arxiv.org/abs/1903.06496>. arXiv:1903.06496 [cs].

Radford, A., Kim, J. W., Hallacy, C., Ramesh, A., Goh, G., and Agarwal, S. Learning transferable visual models from natural language supervision. In *ICML*, pp. 8748–8763. PMLR, 2021a.

Radford, A., Kim, J. W., Hallacy, C., Ramesh, A., Goh, G., Agarwal, S., Sastry, G., Askell, A., Mishkin, P., Clark, J., Krueger, G., and Sutskever, I. Learning Transferable Visual Models From Natural Language Supervision. In *Proceedings of the 38th International Conference on Machine Learning*, pp. 8748–8763. PMLR, July 2021b. URL <https://proceedings.mlr.press/v139/radford21a.html>. ISSN: 2640-3498.

Raghu, M., Gilmer, J., Yosinski, J., and Sohl-Dickstein, J. SVCCA: Singular Vector Canonical Correlation Analysis for Deep Learning Dynamics and Interpretability, November 2017. URL <http://arxiv.org/abs/1706.05806>. arXiv:1706.05806 [stat].

Ramesh, A., Pavlov, M., Goh, G., Gray, S., Voss, C., Radford, A., Chen, M., and Sutskever, I. Zero-shot text-to-image generation. In *ICML*, pp. 8821–8831. PMLR, 2021.

Russakovsky, O., Deng, J., Su, H., Krause, J., Satheesh, S., Ma, S., Huang, Z., Karpathy, A., Khosla, A., Bernstein, M., Berg, A. C., and Fei-Fei, L. ImageNet Large Scale Visual Recognition Challenge. *International Journal of Computer Vision*, 115(3): 211–252, December 2015. ISSN 1573-1405. doi: 10.1007/s11263-015-0816-y. URL <https://doi.org/10.1007/s11263-015-0816-y>.

Schrimpf, M., Kubilius, J., Hong, H., Majaj, N. J., Rajalingham, R., Issa, E. B., Kar, K., Bashivan, P., Prescott-Roy, J., Schmidt, K., Yamins, D. L. K., and DiCarlo, J. J. Brain-Score: Which Artificial Neural Network for Object Recognition is most Brain-Like?, September 2018. URL <https://www.biorxiv.org/content/10.1101/407007v1>. Pages: 407007 Section: New Results.

Singer, U., Polyak, A., Hayes, T., Yin, X., An, J., Zhang, S., and Hu, Q. Make-a-video: Text-to-video generation without text-video data. *arXiv preprint arXiv:2209.14792*, 2022.

Srinivasan, K., Raman, K., Chen, J., Bendersky, M., and Na-jork, M. WIT: Wikipedia-based Image Text Dataset for Multimodal Multilingual Machine Learning. In *Proceedings of the 44th International ACM SIGIR Conference on Research and Development in Information Retrieval*, SIGIR ’21, pp. 2443–2449, New York, NY, USA, July 2021. Association for Computing Machinery. ISBN 978-1-4503-8037-9. doi: 10.1145/3404835.3463257. URL <https://dl.acm.org/doi/10.1145/3404835.3463257>.

Sun, C., Myers, A., Vondrick, C., Murphy, K., and Schmid, C. Videobert: A joint model for video and language representation learning. In *Proceedings of the IEEE/CVF International Conference on Computer Vision*, pp. 7464–7473, 2019.

Thompson, B. Canonical Correlation Analysis. In *Encyclopedia of Statistics in Behavioral Science*. John Wiley & Sons, Ltd, 2005. ISBN 978-0-470-01319-9. doi: 10.1002/0470013192.bsa068.

Tian, Y., Sun, C., Poole, B., Krishnan, D., Schmid, C., and Isola, P. What makes for good views for contrastive learning? *NeurIPS*, 33:6827–6839, 2020.

Tosh, C., Krishnamurthy, A., and Hsu, D. Contrastive learning, multi-view redundancy, and linear models. In *ALT*, 2021.

Touvron, H., Martin, L., Stone, K., Albert, P., Almahairi, A., Babaei, Y., Bashlykov, N., Batra, S., Bhargava, P., Bhosale, S., Bikell, D., Blecher, L., Ferrer, C. C., Chen, M., Cucurull, G., Esiobu, D., Fernandes, J., Fu, J., Fu, W., Fuller, B., Gao, C., Goswami, V., Goyal, N., et al. Llama 2: Open Foundation and Fine-Tuned Chat Models, July 2023. URL <http://arxiv.org/abs/2307.09288>. arXiv:2307.09288 [cs].

Wang, W., Arora, R., Livescu, K., and Bilmes, J. On deep multi-view representation learning. In *ICML*, pp. 1083–1092. PMLR, 2015.

Wightman, R. PyTorch Image Models, 2019. URL <https://github.com/rwightman/pytorch-image-models>. Publication Title: GitHub repository.

Wolf, T., Debut, L., Sanh, V., Chaumond, J., Delangue, C., Moi, A., Cistac, P., Rault, T., Louf, R., Funtowicz, M., Davison, J., Shleifer, S., Platen, P. v., Ma, C., Jernite, Y., Plu, J., Xu, C., Scao, T. L., Gugger, S., Drame, M., Lhoest, Q., and Rush, A. M. Transformers: State-of-the-Art Natural Language Processing. In *Proceedings of the 2020 Conference on Empirical Methods in Natural Language Processing: System Demonstrations*, pp. 38–45, Online, October 2020. Association for Computational Linguistics. URL <https://www.aclweb.org/anthology/2020.emnlp-demos.6>.

Workshop, B., Scao, T. L., Fan, A., Akiki, C., Pavlick, E., Ilić, S., Hesslow, D., Castagné, R., Luccioni, A. S., Yvon, F., Gallé, M., Tow, J., Rush, A. M., Biderman, S., Webson, A., Ammanamanchi, P. S., Wang, T., Sagot, B., Muenninghoff, N., Moral, A. V. d., Ruwase, O., Bawden, R., Bekman, S., McMillan-Major, A., Beltagy, I., Nguyen, H., Saulnier, L., Tan, S., et al. BLOOM: A 176B-Parameter Open-Access Multilingual Language Model, June 2023. URL <http://arxiv.org/abs/2211.05100>. arXiv:2211.05100 [cs].

Xiao, Y., Codevilla, F., Gurram, A., Urfalioglu, O., and López, A. M. Multimodal end-to-end autonomous driving. *IEEE Transactions on Intelligent Transportation Systems*, 23(1):537–547, 2020.

Zadeh, A., Zellers, R., Pincus, E., and Morency, L.-P. MOSI: Multimodal Corpus of Sentiment Intensity and Subjectivity Analysis in Online Opinion Videos, August 2016. URL <http://arxiv.org/abs/1606.06259>. arXiv:1606.06259 [cs].

A. Experimental Details

A.1. Synthetic Data Experiments

On the synthetic dataset, we train MLPs with the AdamW optimizer with the number of hidden dimensions kept the same as the number of input features, 12. For a given level of uniqueness, we choose suitable hyperparameters across different model depths and transformation depths. Specifically, we tune the learning rate in the range $\{1e-1, 1e-2, 1e-3, 1e-4\}$ and weight decay in the range $\{0, 1e-1, 1e-2, 1e-3, 1e-4\}$ for each modality. The depth 1 MLP for the untransformed modality were trained for 50 epochs and the models for the transformed modality were trained for 300 epochs. To ensure robustness, we report results with five different random seeds for each dataset.

A.2. Vision-Language Alignment

We evaluate alignment using the same set of language and vision models as [Huh et al. \(2024\)](#). The language model families considered are BLOOM ([Workshop et al., 2023](#)), OpenLLaMA ([Geng & Liu, 2023](#)), and LLaMA ([Touvron et al., 2023](#)) downloaded from HuggingFace ([Wolf et al., 2020](#)). The vision models are vision transformer models of various sizes trained on various data and objectives. These include classification on ImageNet-21K ([Russakovsky et al., 2015](#)), MAE ([He et al., 2022](#)), DINOv2 ([Oquab et al., 2023](#)), CLIP ([Radford et al., 2021b](#)), and CLIP finetuned on ImageNet-12K. These models were downloaded from PyTorch Image Models ([Wightman, 2019](#)).

A.3. MultiBench Experiments

We train transformers on the pre-extracted video, audio, and text features for the affective computing datasets and the audio modality of AVMNIST, and vision transformers on the AVMNIST digit images. For each modality, we vary the depth of the transformers in the range $\{1, \dots, 10\}$. We use a single head for self-attention and set the embedding size to the input dimension. For classification tasks, we append a `[cls]` token to the sequence with a learnable embedding. The embedding of this token is used to compute alignment between layers; otherwise, we do average pooling over the input sequence. We use the AdamW optimizer. For each dataset, we choose suitable hyperparameters across different model depths and tune the learning rate in the range $\{1e-3, 5e-4, 1e-4, 5e-5, 1e-5\}$ and weight decay in the range $\{0, 1e-1, 1e-2, 1e-3, 1e-4\}$.

To ensure robustness, we train each architecture across 3 different seeds, providing 30 alignment-performance data points. To get the alignment-performance correlation given modalities 1 and 2, the alignment of every modality 2 model is computed with respect to the modality 1 model with the highest validation score across the different seeds, and we report the correlation of these alignment scores with the performance of the modality 2 models.

B. Alignment Computation

Given mean-centered feature sets of n samples, $Z_1, Z_2 \in \mathbb{R}^{n \times d}$, from two modalities X_1 and X_2 , we first compute the covariances of these two different feature sets, and then compute the empirical estimator of the Hilbert-Schmidt Independence Criterion ([Gretton et al., 2005](#)) using a linear kernel. Hence,

$$\text{HSIC}(Z_1 Z_1^T, Z_2 Z_2^T) = \frac{1}{(n-1)^2} \text{Tr}(Z_1 Z_1^T Z_2 Z_2^T) = \frac{1}{(n-1)^2} \|Z_1^T Z_2\|_F^2 \quad (1)$$

The Centered Kernel Alignment (CKA) ([Kornblith et al., 2019](#)) is then obtained by normalizing HSIC to ensure scale invariance and comparability across different feature sets:

$$\text{CKA}(Z_1, Z_2) = \frac{\text{HSIC}(Z_1 Z_1^T, Z_2 Z_2^T)}{\sqrt{\text{HSIC}(Z_1 Z_1^T, Z_1 Z_1^T) \text{HSIC}(Z_2 Z_2^T, Z_2 Z_2^T)}} \quad (2)$$

As demonstrated in ([Huh et al., 2024](#)), the definition of alignment can be adjusted to limit the cross-covariance measurement to only those samples identified as nearest neighbors of the current sample i . This modification prioritizes similarity over dissimilarity, thereby emphasizing local alignment:

$$\text{ALIGN}_{\text{MKNN}}(Z_1, Z_2) = \sum_i \sum_j \alpha(i, j)) \quad (3)$$

$$\text{where, } \alpha(i, j) = \mathbf{1}[Z_{1,j} \in \text{knn}(Z_{1,i}) \wedge Z_{2,j} \in \text{knn}(Z_{2,i}) \wedge i \neq j] \quad (4)$$

Here, $Z_{1,k}$ and $Z_{2,k}$ refer to the k^{th} row of Z_1 and Z_2 , respectively, while MKNN denotes Mutual KNN.

Thus, Mutual-KNN MKNN is defined as:

$$\text{MKNN}(Z_1, Z_2) = \frac{\text{ALIGN}_{\text{MKNN}}(Z_1, Z_2)}{\sqrt{\text{ALIGN}_{\text{MKNN}}(Z_1, Z_1) \cdot \text{ALIGN}_{\text{MKNN}}(Z_2, Z_2)}} \quad (5)$$

Following [Huh et al. \(2024\)](#), we use $k = 10$ nearest neighbors over 1024 samples from the Wikipedia caption dataset. For the vision model, the class token of each layer is used, and for the language model, the embeddings of a given layer are average pooled to a single token. l_2 normalization is applied to the features and elements in the features that are above the 95-th percentile are truncated.

After computing the alignment between all pairs of layers between E_1 and $E_{2,d}$ using CKA or mutual KNN, we report the best alignment score across all layer pairs ([Schimpf et al., 2018](#)).

C. Dataset Details

C.1. Synthetic Data

We discuss in detail how we construct a synthetic dataset with two modalities to analyze how uniqueness, redundancy, and heterogeneity influence the emergence of alignment. Let $x_1 = [x_r, x_{u_1}]$ and $x_2 = [x_r, x_{u_2}]$. Here, $x_r \in \mathbb{R}^{n_R}$ represents the redundant information shared between the two modalities, while $x_{u_1}, x_{u_2} \in \mathbb{R}^{n_U}$ denote the unique information for each modality. Both x_1 and x_2 represent arbitrary data samples.

For each data sample, we generate x_r , x_{u_1} , and x_{u_2} by sampling binary vectors from a uniform distribution. Specifically, $x_r \sim \text{Uniform}(\{0, 1\}^{n_R})$, $x_{u_1} \sim \text{Uniform}(\{0, 1\}^{n_U})$, and $x_{u_2} \sim \text{Uniform}(\{0, 1\}^{n_U})$.

To define the labels for this dataset, we introduce task masks $M_R \in \mathbb{R}^{n_R}$ and $M_{U_1}, M_{U_2} \in \mathbb{R}^{n_U}$, which determine the features used in computing the output labels. These masks indicate whether a particular feature contributes to the label-generation process. Specifically, the task masks are defined as follows, where the subscript i refers to the i^{th} entry of the respective mask vector:

$$M_{R_i} = \begin{cases} 1 & \text{if } 0 \leq i < n_R, \\ 0 & \text{otherwise.} \end{cases} \quad (6)$$

$$M_{U_{1,i}} = \begin{cases} 1 & \text{if } 0 \leq i < \lceil \frac{n_U}{2} \rceil, \\ 0 & \text{otherwise.} \end{cases} \quad (7)$$

$$M_{U_{2,i}} = \begin{cases} 1 & \text{if } 0 \leq i < \lfloor \frac{n_U}{2} \rfloor, \\ 0 & \text{otherwise.} \end{cases} \quad (8)$$

We define the task label y as a function $\psi_Y(\cdot)$ of the masked components $x_r \odot M_R$, $x_{u_1} \odot M_{U_1}$, and $x_{u_2} \odot M_{U_2}$, such that:

$$y = \psi_Y(x_r \odot M_R, x_{u_1} \odot M_{U_1}, x_{u_2} \odot M_{U_2}), \quad (9)$$

where $x_r \odot M_R$ captures the task-relevant redundant information, $x_{u_1} \odot M_{U_1}$ captures the task-relevant unique information from modality 1 and $x_{u_2} \odot M_{U_2}$ captures the task-relevant unique information from modality 2.

Here, \odot denotes the element-wise (Hadamard) product. Intuitively, the task masks M_R , M_{U_1} , and M_{U_2} are essential for controlling the relative contributions of the redundant (x_r) and unique (x_{u_1}, x_{u_2}) components to the label generation process.

In our synthetic experiments, we assume the joint distribution of the components as follows:

$$\mathbb{P}(X_C, X_{U_1}, X_{U_2}) = \mathbb{P}(X_C)\mathbb{P}(X_{U_1})\mathbb{P}(X_{U_2}) \quad (10)$$

$$\text{Where, } \mathbb{P}(X_C) = \text{Uniform}(\{0, 1\}^{n_R}) \quad (11)$$

$$\mathbb{P}(X_{U_1}) = \text{Uniform}(\{0, 1\}^{n_U}) \quad (12)$$

$$\mathbb{P}(X_{U_2}) = \text{Uniform}(\{0, 1\}^{n_U}) \quad (13)$$

This formulation assumes that the redundant information (x_r) and the unique components (x_{u_1}, x_{u_2}) are all independently distributed.

The task masks play a critical role in modulating which features are used to compute the labels, thereby allowing precise control over the relative importance of shared and unique information in the synthetic dataset. This design facilitates the study of how these components influence alignment and downstream task performance.

In our experiments, we fix n_Y (the number of features relevant for the task) while varying n_R, n_U to explore different dataset configurations. Concretely, $n_Y = n_R + n_U$.

When $n_y = n_R$, both modalities have equal amounts of task-relevant information, allowing them to perform equally well on the downstream classification task. However, when $n_R < n_Y$, the shared information x_c becomes insufficient to fully capture the task-relevant features. By adjusting the proportion of $\frac{n_R}{n_Y}$, we heuristically vary the amount of task-specific shared information. This allows us to explore how the balance of redundant and unique information impacts alignment and downstream performance.

An example of this is when $n_Y = 2$, $x_r \sim \text{Uniform}(\{0, 1\})$, $x_{u_1} \sim \text{Uniform}(\{0, 1\})$, $x_{u_2} \sim \text{Uniform}(\{0, 1\})$. Given that the label function is an OR function of $[x_r, x_{u_1}]$, where $n_U = 1$, we can see how the label predictions would differ based on $x_1 = [x_r, x_{u_1}]$ and $x_2 = [x_r, x_{u_2}]$ in Table 2.

x_1	x_2	\hat{y}_1	\hat{y}_2	y
00	00	0	0	0
01	00	1	0	1
00	01	0	0	0
01	01	1	0	1
10	10	1	1	1
11	10	1	1	1
10	11	1	1	1
11	11	1	1	1

Table 2: $n_U = 1$ **Predictions.** \hat{y}_2 is incorrect for 2 examples due to lacking the unique information.

In contrast, when the labels are an OR of $[x_{u_1}, x_{u_2}]$, where $n_U = 2$, we can see how the label predictions would differ based on $x_1 = [x_r, x_{u_1}]$ and $x_2 = [x_r, x_{u_2}]$ in Table 3.

x_1	x_2	\hat{y}_1	\hat{y}_2	y
00	00	0	0	0
01	00	1	0	1
00	01	0	1	1
01	01	1	1	1
10	10	0	0	0
11	10	1	0	1
10	11	0	1	1
11	11	1	1	1

Table 3: $n_U = 2$ **Predictions.** Both \hat{y}_1 and \hat{y}_2 are incorrect for 2 examples due to lacking unique information in the other modality.

To incorporate heterogeneity into the setup, we transform the second modality (x_2) using a nonlinear function $\phi(\cdot)$.

Specifically, $\phi(\cdot)$ is modeled as a multilayer perceptron (MLP), where the number of layers (D_ϕ), also referred to as transformation depth, serves as a heuristic measure of heterogeneity. A higher D_ϕ implies a more complex transformation, thereby increasing the heterogeneity between the two modalities. Hence, concretely, $x_{2,\phi} = \phi([x_c, x_{u_2}])$.

In all our experiments, we fix $n_Y = 8$, which represents the total number of task-relevant features. We vary $n_R \in \{0, \dots, 8\}$, thereby controlling the amount of redundant (shared) task-specific information. Consequently, the amount of unique task-specific information is determined as $n_U = n_Y - n_R$. We refer to the level of unique information as $U = n_U$.

C.2. MultiBench Dataset

Below, we discuss the MultiBench datasets in more detail.

- **MUSTARD** (Castro et al., 2019) is a dataset for automated sarcasm discovery, compiled from popular TV shows, including Friends, The Golden Girls, The Big Bang Theory, and Sarcasmaholics Anonymous. There are 414, 138, and 138 video segments in the training, validation, and testing data, which gives a total of 690 data points.
- **MOSI** (Zadeh et al., 2016) is a dataset for sentiment analysis consisting of 2,199 opinion video clips. Each video is further split into short segments (roughly 10-20 seconds) that are annotated, resulting in 1284, 229, 686 segments in the train, validation, and testing sets. As the annotations are sentiment intensity, which ranges from [-3, 3], we train our models on the continuous labels with L1 loss and evaluate positive-negative classification accuracy.
- **UR-FUNNY** (Hasan et al., 2019) is a large-scale dataset for humor detection in human speech, consisting of more than 16000 video samples (from TED talks collected from 1866 videos. There are a total of 10,598, 2,626, and 3,290 segments in the train, validation, and testing sets. Humor is annotated as either positive or negative, with a homogeneous 50% split in the dataset.
- **MOSEI** (Bagher Zadeh et al., 2018) is a large-scale dataset for sentence-level sentiment analysis and emotion recognition from real-world online videos, containing more than 65 hours of annotated video from more than 1,000 speakers and 250 topics. There are a total of 16,265, 1,869, and 4,643 segments in the train, validation, and testing sets, resulting in 22,777 data points. As in MOSI, we train our models on continuous sentiment intensity labels with L1 loss and evaluate positive-negative classification.
- **AVMNIST** (Pérez-Rúa et al., 2019) is a dataset created by pairing audio of a human reading digits from the FSDD dataset (Jackson, 2025) with written digits in the MNIST dataset (Lecun et al., 1998) with a task to predict the digit into one of 10 classes (0-9). While common practice (Pérez-Rúa et al., 2019) is to increase difficulty by removing 75% of energy in the visual modality via PCA and adding noise from ESC-50 to the audio modality, we use the unnoised image and audio modalities in order to preserve the redundant information between modalities. An audio sample from FSDD with matching digit identity is paired with each image in MNIST, resulting in 55000, 5000, and 10000 examples in the train, validation, and test sets respectively. We train vision transformers on MNIST images that are converted to 4x4 patches with a sequence length of 49. We preprocess the raw FSDD audio into 36 MFCC coefficients with a maximum sequence length of 20 using librosa (McFee et al., 2015).

D. Additional Figures

D.1. Additional Synthetic Data Results

In Figures 10, we plot the alignment between unimodal encoders over the levels of heterogeneity, demonstrating that the maximum alignment negatively correlates with heterogeneity.

In Figures 11, 12, and 13, we plot the relation between alignment and performance for individual synthetic datasets, which show that as uniqueness increases, alignment is no longer an indicator of performance.

D.2. Vision-Language Alignment vs Unique

In Figures 14, 15, 16, and 17, we plot the relation between vision-language alignment and uniqueness, which show that the maximum alignment decreases with uniqueness.

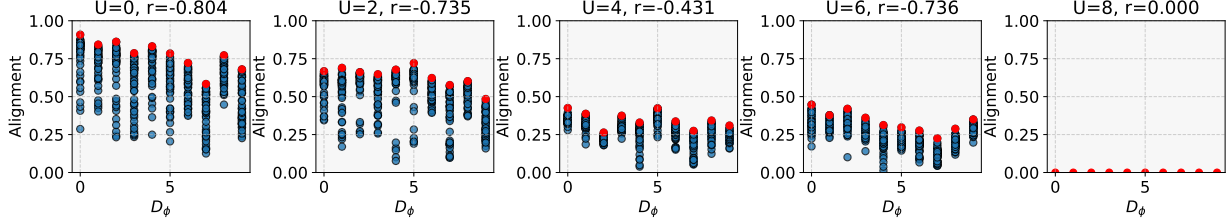


Figure 10: **Alignment vs. Heterogeneity.** The alignment is computed between unimodal encoders trained on datasets with different levels of heterogeneity. Each dot is an independent run on a different model size on a given dataset. We compute the Pearson correlation coefficient r between heterogeneity and maximum alignment, and see that the maximum level of achievable level of alignment decreases as the level of uniqueness increases. 5 different figures shows 5 levels of informational uniqueness.

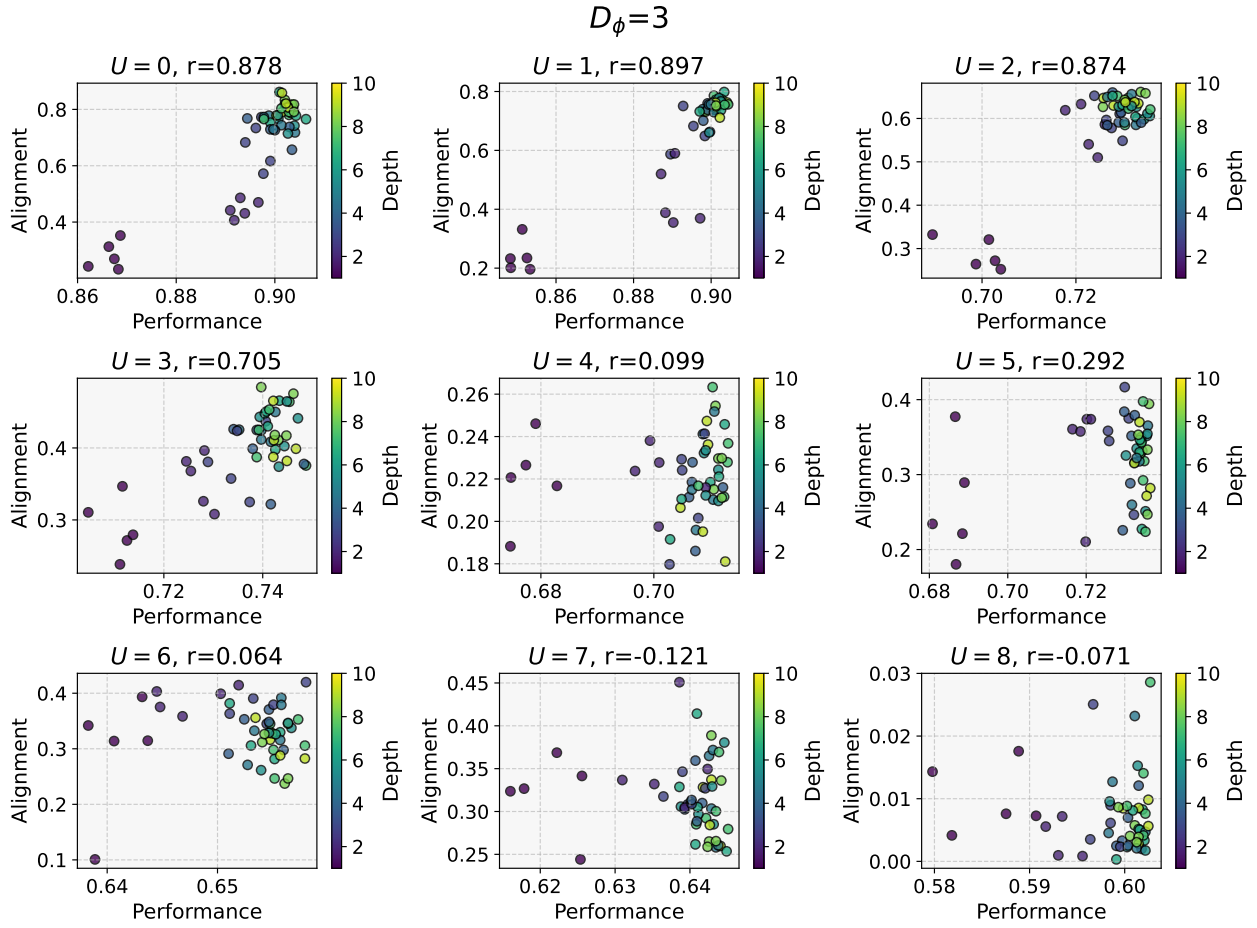


Figure 11: **Alignment vs Performance for $D_\phi = 3$.** The alignment-performance trend is shown across different levels of uniqueness, with the Pearson's correlation coefficient r reported for each plot.

D.3. Vision-Language Alignment vs Performance

In Figures 18, 19, 20, 21, and 22, we plot the relation between vision-language alignment and performance.

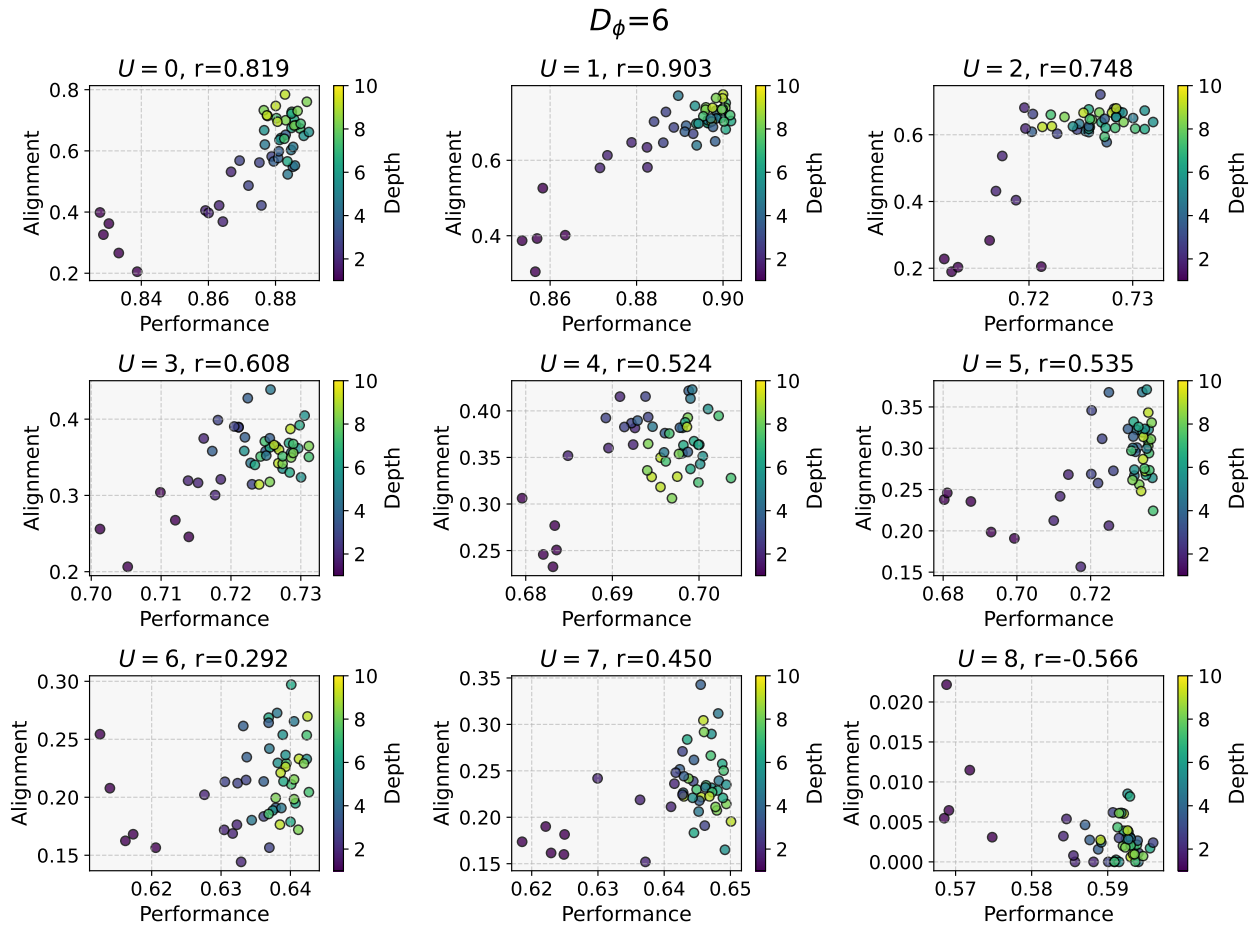


Figure 12: **Alignment vs Performance for $D_\phi = 6$.** The alignment-performance trend is shown across different levels of uniqueness, with the Pearson's correlation coefficient r reported for each plot.

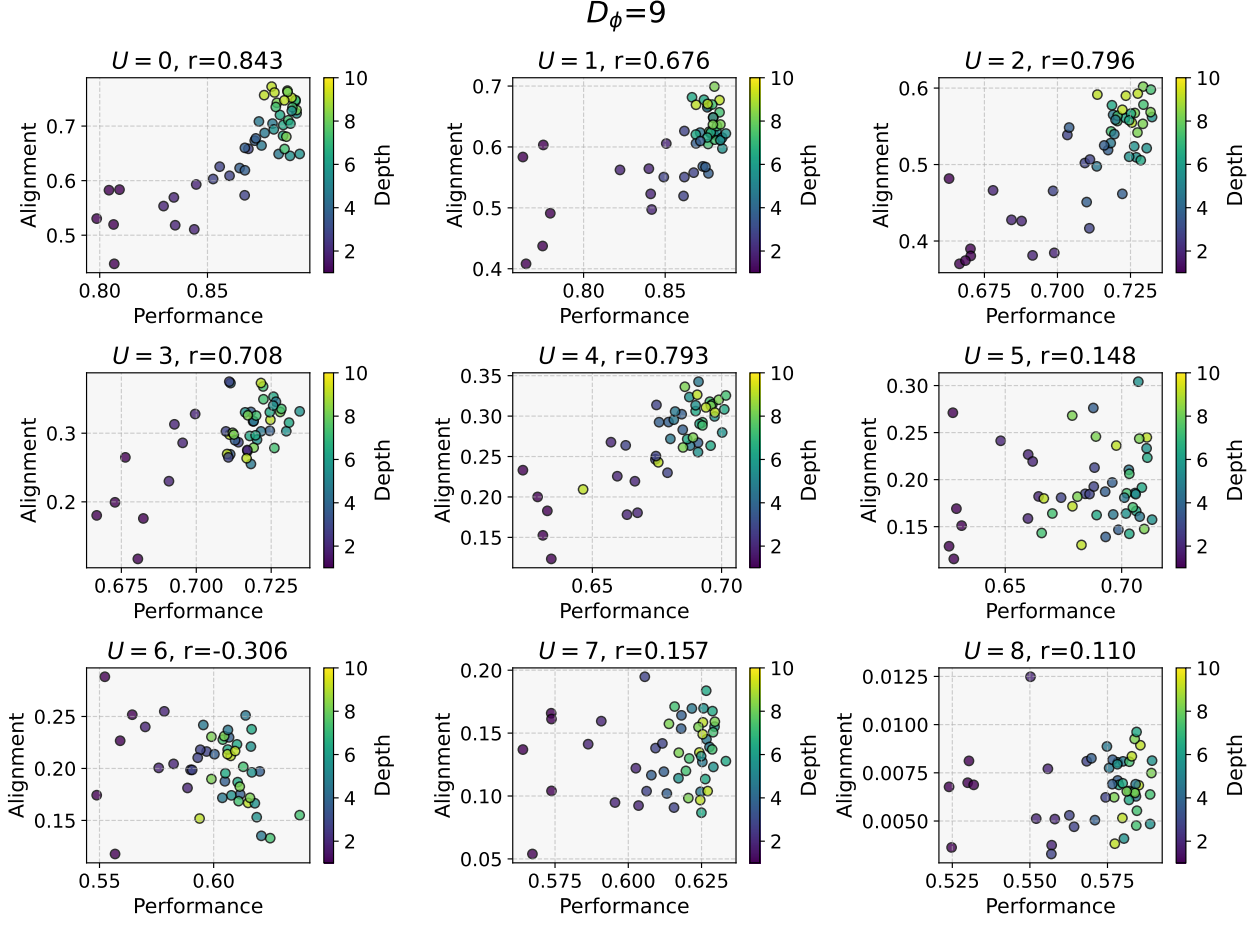


Figure 13: **Alignment vs Performance for $D_\phi = 9$** . The alignment-performance trend is shown across different levels of uniqueness, with the Pearson’s correlation coefficient r reported for each plot.

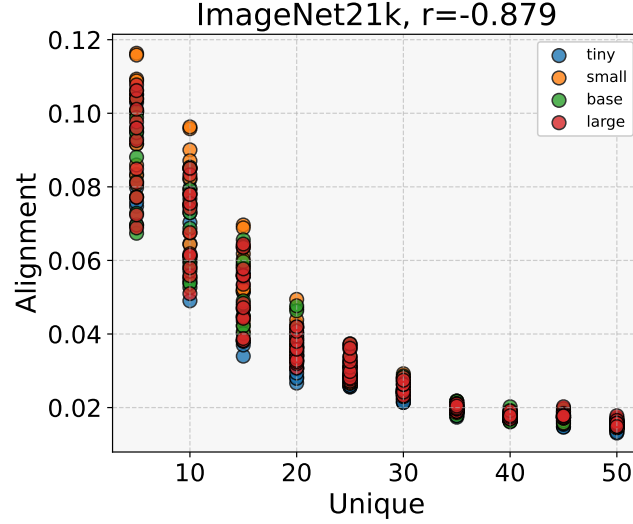


Figure 14: **ImageNet21k Alignment vs Uniqueness**. The alignment is computed between vision models trained on ImageNet21k and large language models. We compute the Pearson correlation coefficient r between the maximum alignment and uniqueness.

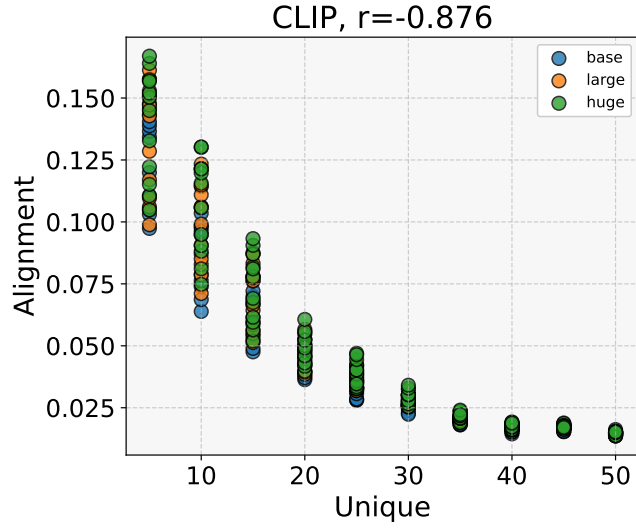


Figure 15: **CLIP Alignment vs Uniqueness.** The alignment is computed between CLIP vision models and large language models. We compute the Pearson correlation coefficient r between the maximum alignment and uniqueness.

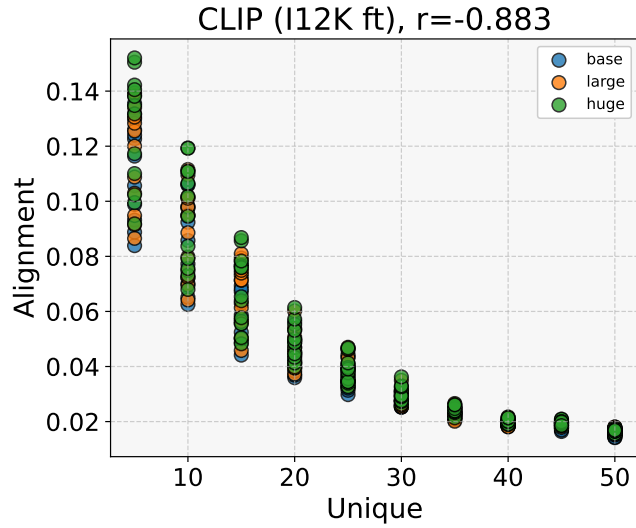


Figure 16: **CLIP Finetuned on ImageNet21k Alignment vs Uniqueness.** The alignment is computed between vision models trained with CLIP and finetuned on ImageNet21k and large language models. We compute the Pearson correlation coefficient r between the maximum alignment and uniqueness.

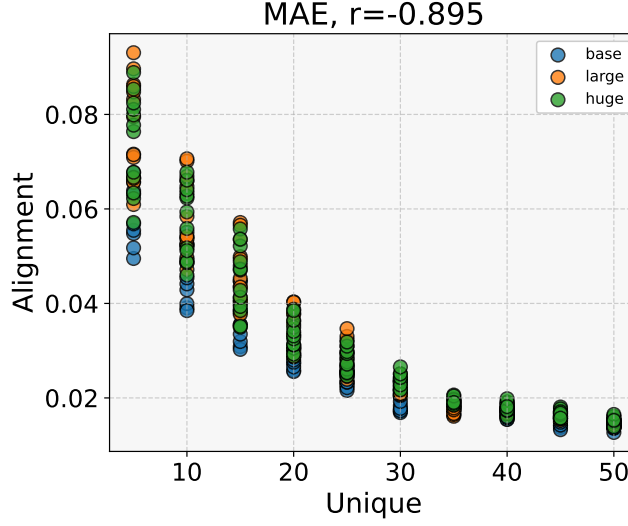


Figure 17: **MAE Alignment vs Uniqueness.** The alignment is computed between MAE vision models and large language models. We compute the Pearson correlation coefficient r between the maximum alignment and uniqueness.

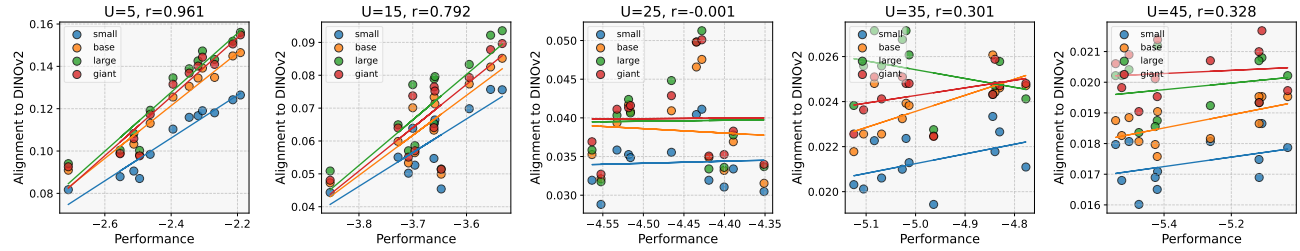


Figure 18: **DINOv2 Vision-Language Alignment vs Performance.** We plot the vision-language alignment using DINOv2 vision models with respect to language model performance, measured using bits-per-byte-loss and show individual best fit lines for each size of vision model as well as the average Pearson correlation coefficient r .

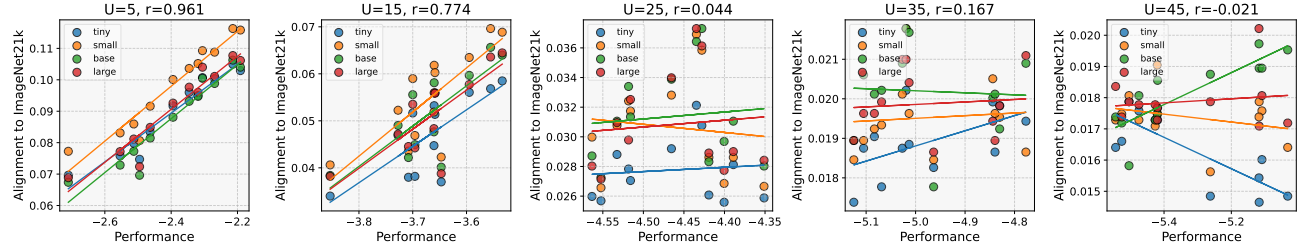


Figure 19: **ImageNet21K Vision-Language Alignment vs Performance.** We plot the vision-language alignment using vision models trained on ImageNet21K classification with respect to language model performance, measured using bits-per-byte-loss and show individual best fit lines for each size of vision model as well as the average Pearson correlation coefficient r .

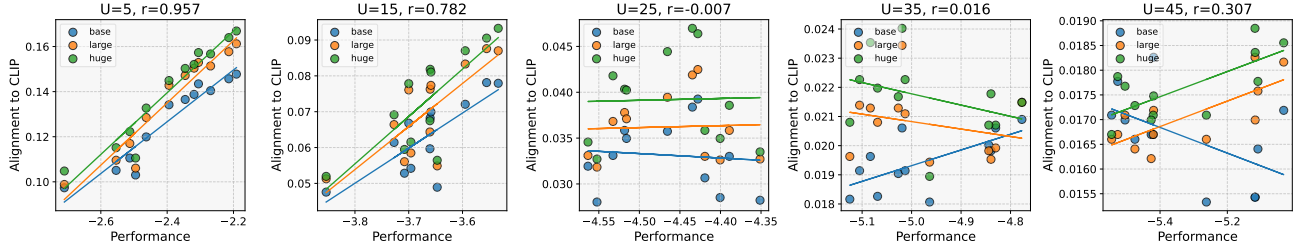


Figure 20: **CLIP Vision-Language Alignment vs Performance.** We plot the vision-language alignment using CLIP vision models with respect to language model performance, measured using bits-per-byte-loss and show individual best fit lines for each size of vision model as well as the average Pearson correlation coefficient r .

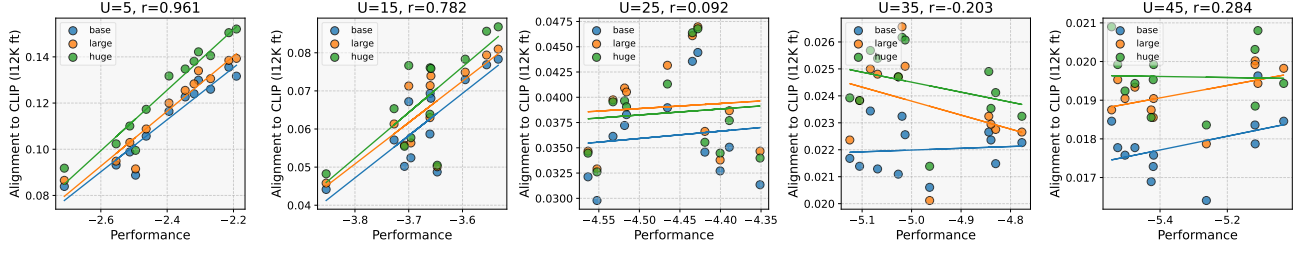


Figure 21: **CLIP finetuned on ImageNet-21k Vision-Language Alignment vs Performance.** We plot the vision-language alignment using CLIP finetuned on ImageNet-21k vision models with respect to language model performance, measured using bits-per-byte-loss and show individual best fit lines for each size of vision model as well as the average Pearson correlation coefficient r .

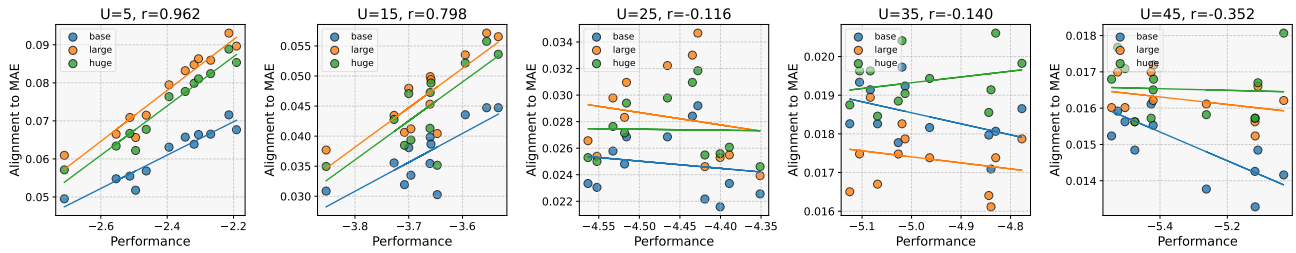


Figure 22: **MAE Vision-Language Alignment vs Performance.** We plot the vision-language alignment using MAE vision models with respect to language model performance, measured using bits-per-byte-loss and show individual best fit lines for each size of vision model as well as the average Pearson correlation coefficient r .